Journal of Alloys and Compounds 579 (2013) 372–376

Contents lists available at SciVerse ScienceDirect

Journal of Alloys and Compounds

journal homepage: www.elsevier.com/locate/jalcom

In situ synthesis of CoS_2/RGO nanocomposites with enhanced electrode performance for lithium-ion batteries

Bin Qiu [a], Xiuyun Zhao [a], Dingguo Xia [b,*]

[a] College of Environmental & Energy Engineering, Beijing University of Technology, Beijing 100124, China
[b] Key Laboratory of Theory and Technology of Advanced Battery Materials, College of Engineering, Peking University, Beijing 100871, China

ARTICLE INFO

Article history:
Received 4 March 2013
Received in revised form 27 April 2013
Accepted 22 May 2013
Available online 25 June 2013

Keywords:
Lithium ion batteries
Anode
Reduced graphene oxides
CoS_2

ABSTRACT

This study reports a novel strategy of preparing CoS_2/reduced graphene oxides (RGO) nanocomposites by employing graphene oxides (GO) as an oxidizing agent and $Na_2S_2O_3$ as a reducing agent. CoS_2 can be in situ synthesized with GO being reduced. X-ray diffraction (XRD), Raman spectrometry, scanning electron microscopy (SEM), transmission electron microscopy (TEM) and electrochemical test are used to characterize the nanocomposite. The CoS_2 particles with the size of 150 nm are dispersed in the networks made from thin RGO nanosheets. The CoS_2/RGO nanocomposite as an anode material for lithium-ion batteries can deliver excellent reversible capacity retention (640 mA hg^{-1}) after cycling 50 times when tested at 100 mA g^{-1} and rate performance. The enhanced electrochemical properties can be attributed to the nanoscale particles sizes of CoS_2 in addition to the effects of RGO networks in preventing the agglomeration of CoS_2 and absorbing lithium polysulfides during the charge-discharge processes.

1. Introduction

Lithium ion batteries have attracted considerable attentions with the development of mobile electronics and electric vehicles [1]. Numerous studies are focused on electrode materials, separators, and electrolytes [2,3]. Particularly, the anode material is regarded as one of the key elements in the construction of high capacity lithium ion batteries. Since Poizot et al. first reported the mechanism of transition oxides and sulfides [4], metal sulfides have attracted great attention due to its high theoretical capacity (much higher than that of graphite ~372 mA hg^{-1}) and low cost [5,6]. In particular, cobalt sulfides (CoS, CoS_2, Co_3S_4, Co_9S_8, etc.) are widely investigated and much progress has been made in Li-ion storage capacities [7–12]. However, according to some previous reports [13,14], the Li storage process in the conversion reaction based metal sulfides involves generation of polysulfides Li_2S_x ($2 < x < 8$). The dissolved lithium polysulfides shuttle between the anode and cathode during the charge process, involving side reduction reactions with lithium anode and reoxidation reactions at the cathode, which decrease the columbic efficiency and cause a poor cyclability of LIBs. In order to solve these problems, two main kinds of strategies are adopted. First, some reports are focused on designing special structures (hollow spheres, polyhedral spheres) [15,16]. The special structure of the electrode materials is believed to facilitate the diffusion of lithium ions [17]. The second is carbon coating [18], in which carbon acts as a layer to buffer large volume changes, mitigates the aggregation of particles and increases the electronic conductivity of electrodes [19].

Graphene, as a single two dimensional layer of carbon atoms, is a good candidate to host active NPs for Li ion batteries because of its high stability, large surface areas, and abundant functional groups [20]. Various hybrid nanostructures containing graphene nanosheet have been extensively studied as electrode materials in recent years [21–24]. In order to increase its electrical conductivity as electrode materials for lithium ion batteries, the GO need reduction treatment in special reducing atmosphere [25,26], which is usually harsh and tedious.

Herein, we propose a novel method to prepare CoS_2/RGO by employing graphene oxides (GO) as an oxidizing agent and $Na_2S_2O_3$ as a reducing agent. The CoS_2 particles of about 150 nm were highly uniform dispersed on RGO nanosheets. When used as anode material for lithium ion batteries, CoS_2/RGO composites exhibit good cycling stability and rate capability.

2. Experimental

2.1. Synthesis of CoS_2/RGO composites

In a typical synthesis, 2.5 mmol of $CoCl_2 \cdot 6H_2O$ was dissolved in deionized water (60 mL) at room temperature for 2 h. Then the blue solution was transferred into a 100 mL Teflon-lined stainless steel autoclave followed by the addition of 2.5 mmol of $Na_2S_2O_3 \cdot 5H_2O$ and 20 mL GO and subsequently agitated it for 2 h. The sealed tank was maintained at 150 °C for 12 h. After reaction, the autoclave was cooled to room temperature. The black product was harvested by filtration and washed with CS_2, ethanol, de-ionized water before drying at 80 °C overnight. For comparison, pristine CoS_2 was prepared following the similar procedures in the absence of GO [27,28].

* Corresponding author. Tel.: +86 10 62767962; fax: +86 10 62768316.
E-mail address: dgxia@pku.edu.cn (D. Xia).

0925-8388/$ - see front matter © 2013 Elsevier B.V. All rights reserved.
http://dx.doi.org/10.1016/j.jallcom.2013.05.148

2.2. Characterization

The obtained products were characterized by X-ray diffraction (XRD, BRUKER D8 ADVANCED, Cu Kα = 1.54 Å) with a scan rate of 0.02° S^{-1} from 10° to 80°. The operating voltage and current were kept at 40 kV and 40 mA, respectively. The size and morphology of the as-synthesized products were examined by using a scanning electron microscope (SEM-HITACHI S-4800) and transmission electron microscope (JEOL 2010). Raman spectroscopic analysis was performed with a LabRAM HR800 with laser excitation energy of 632.8 nm. Fourier transform infrared spectroscopy (FTIR) was collected by a Thermo Fisher spectrophotometer using the KBr pellet method. Thermogravimetric analysis (TGA) was carried out on a TG/DTA7300 thermal analyzer with a heating rate of 5 °C min^{-1} in flowing air atmosphere.

2.3. Cell assembly and testing

The working electrode was composed of active material (60 wt%), Super P (30 wt%) and poly(vinylidene difluoride) (PVDF, 10 %wt). These materials were mixed in N-methyl pyrrolidone to form homogenous slurry. Then the slurry was spread onto the nickel foam and dried under vacuum at 120 °C for 12 h. After the drying process, the foam was pressed under a pressure of 20 MPa. The coin cells were finally assembled in an argon filled glovebox with the as-prepared materials as test electrode, metallic lithium as the counter and referenced electrode, 1 M $LiPF_6$ in EC:DMC (1:1 in volume)as the electrolyte, and Whatman GF/D borosilicate glass-fiber sheets as separator, respectively. Coin cells were cycled galvanostatically in the voltage range between 0.02 and 3.00 V at a current density of 100 mA g^{-1} with a multichannel battery test system (NEWARE).

3. Results and discussion

Fig. 1a shows the power X-ray diffraction (XRD) patterns of the as-synthesized CoS_2 and CoS_2/RGO. The dominant diffraction peaks of both samples correspond to CoS_2, which can be indexed to the standard cubic phase CoS_2 (JCPDS Card No. 65-3322) with a space group of Pa-3 (205). No obvious peaks relevant with Co and S can be found in the patterns. CoS_2/RGO is further evaluated from TG analysis, as shown in Fig. 1b. The main weight loss is between 400 K and 800 K, indicating the complete combustion of RGO. It can be deduced that the content of RGO in CoS_2/RGO is about 20% according to TG analysis.

CoS_2/RGO composite is further characterized by Raman and FTIR spectroscopy, as shown in Fig. 2. Fig. 2a shows FTIR spectra of GO, CoS_2, and CoS_2/RGO, respectively. FTIR spectra verifies the presence of some oxygen–containing groups in GO, such as C—OH (3390 cm^{-1}), C—O—C (1230 cm^{-1}), the C—O stretching peak (1055 cm^{-1}) and C=O in carboxylic acid moieties (1730 cm^{-1}). The peak at 1620 cm^{-1} is assigned to the contribution from the skeletal vibrations of the graphitic domains [29]. There is no obvious peak around 3390 cm^{-1} and 1730 cm^{-1} for CoS_2/RGO, which means that GO was reduced, while the strong peak around 1060 cm^{-1} is attributed to Co=S stretching in CoS_2 [30], another weak peak around 1571 cm^{-1} was assigned to aromatic C=C group [31]. In Fig. 2b, CoS_2/RGO exhibits two typical peaks at 1350 and 1580 cm^{-1}, which are the characterized peaks of the disorder (*D*) and graphite (*G*) bands of graphene sheets [32]. It is generally accepted that the I_D/I_G ratio reflects the graphitization of carbonaceous materials and also the defect density [33]. The intensity ratio of the *D* to *G* band (I_D/I_G) are 1.1 and 1.27 for GO and CoS_2/RGO. It is obvious that I_D/I_G for CoS_2/RGO increases slightly compared with GO, which may be ascribed to the presence of $Na_2S_2O_3$, which can be used as reducing agents to reduce graphene oxides to graphene [34]. Because $Na_2S_2O_3$ is environmental friendly, easy to obtain, and stable in ambient conditions, this strategy to prepare CoS_2/RGO in this work is more suitable for large scale synthesis [27].

To investigate the size and morphology of the samples, SEM, TEM, and HR-TEM were collected for CoS_2 and CoS_2/RGO in (Fig. 3d). The SEM image taken from a typical section of CoS_2/RGO (Fig. 3a) indicates the size of uniformly dispersed CoS_2 particles anchored on RGO nanosheets to be about 150 nm. In comparison with CoS_2/RGO, CoS_2 particles in the absence of RGO (Fig. 3b) show heavily particles aggregation that means RGO nanosheets play an essential role in achieving good dispersion of the CoS_2 NPs. The origin of smaller particles and lower aggregation for CoS_2/RGO can be analyzed in the following. There are many functional groups such as C=O, O—C=O, and C—O containing negative charges favor the absorbing of Co^{2+} on GO [35]. The cobalt ions are selectively and uniformly anchored onto GO's surface. In other words, the functional groups act as nucleation sites for CoS_2 NP

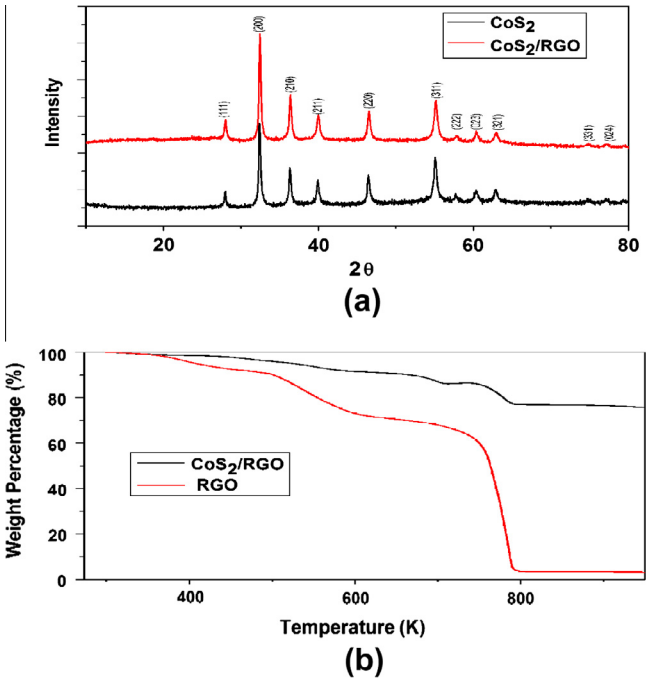

Fig. 1. (a) XRD pattern of CoS_2, and CoS_2/RGO. (b) Thermogravimetric (TG) result of CoS_2/RGO and RGO in air with a heating rate of 5 °C/min.

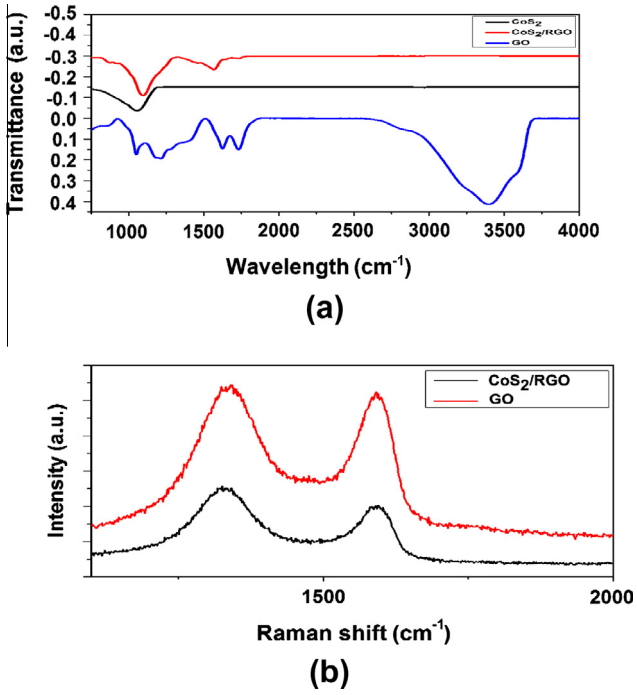

Fig. 2. (a) FTIR spectra of GO, CoS_2, CoS_2/RGO. (b) Raman spectra of CoS_2/RGO and GO.

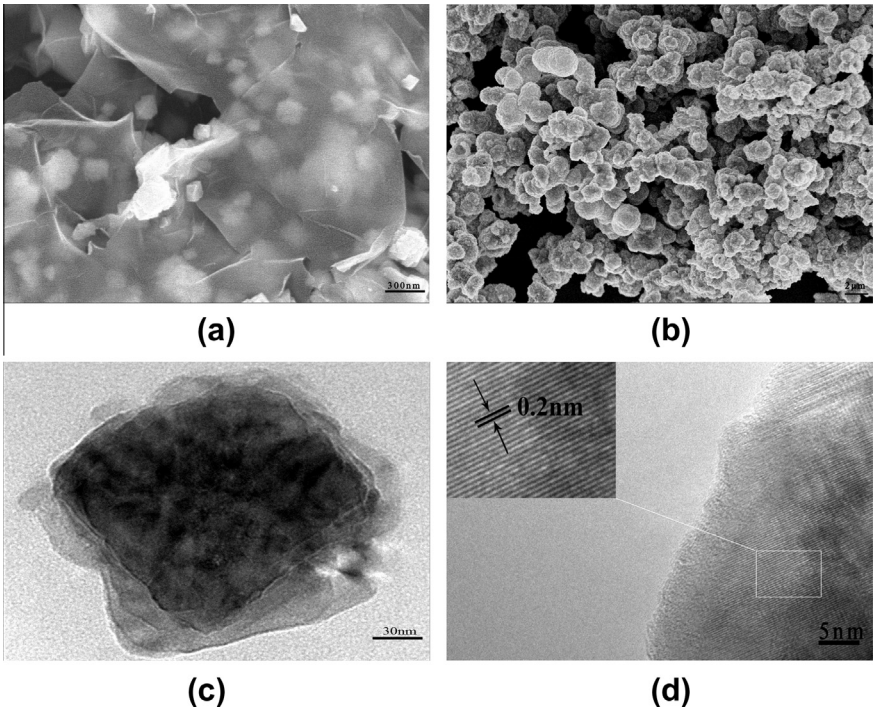

Fig. 3. (a) SEM images of CoS_2/RGO. (b) SEM images of CoS_2. (c) TEM images of CoS_2/ RGO. (d) High-resolution TEM (HRTEM) image of CoS_2/RGO.

nucleation. The homogeneous nucleation and growth in the bulk solution are suppressed so that small CoS_2 particles can be obtained. TEM images of noncomposites are shown in Fig. 3c. it is clear that the particle size of CoS2 is consistent with SEM images. In the high-resolution TEM image of CoS_2/RGO (Fig. 3d), crystalline planes of CoS_2 (200) with a distance spacing of 0.2 nm can be clearly observed, which is in accordance with XRD pattern.

The electrochemical performance of CoS_2 and CoS_2/RGO electrode are investigated by galvanostatic discharge-charge technique. Fig. 4a shows the discharge–charge voltage profiles cycled at a current density of 100 mA g^{-1} between 0.02 and 3.0 V vs. Li^+/Li. The plateau at 1.5 V is ascribed to the formation of Li_xCoS_2 [36]. While the voltage is further decreased, the plateau at 1.0 V is followed by a long slope corresponding to the conversion reaction and the formation of SEI film on the surface of the electrode [15]. The initial charge and discharge capacity of CoS_2/RGO are 812 mA hg^{-1} and 1344 mA hg^{-1}, respectively, based on the total mass of the CoS_2/RGO nanocomposite with an irreversible capacity loss of 39.6%. Fig. 4b shows the first charge and discharge capacity of CoS_2 were 823 mA hg^{-1} and 1197 mA hg^{-1}, respectively, with an irreversible capacity loss is about 31%. The large initial discharge capacity of the CoS_2/RGO could be attributed to the formation of SEI during the discharge process and the irreversible decomposition of Li_2S [37]. In addition, the graphene networks with high surface area and many oxygen-containing groups may also contribute to this issue [38]. Though a large irreversible capacity loss was observed in the first cycle, CoS_2/RGO nanocomposites exhibit a higher specific capacity and better cycling stability in comparison with the pristine CoS_2. Indeed, Li intercalation into the RGO was also observed in the Fig. 4. We think that the calculation of capacity based on total active mass (CoS_2 and RGO) is of more practical significance. In order to discern the contribution of RGO and CoS_2, the as-prepared pristine CoS_2 and RGO were evaluated as shown in Fig. 4b and c, respectively. The pristine CoS_2 electrode remained a reversible capacity of only 250 mA hg^{-1} and as-prepared RGO electrode showed a reversible capacity of 150 mA hg^{-1}. In contrast, the capacity keeps at the level of 690 mA hg^{-1} after 20 cycles as shown in Fig. 4a. Therefore, the enhanced reversible capacity of CoS_2/RGO composite electrode can be ascribed to the synergic effects of RGO and CoS_2. Furthermore, after 50 cycles under a current density of 100 mA g^{-1}, the CoS_2/RGO nanocomposites still retain a reversible capacity of ~640 mA hg^{-1} with an average coulombic efficiency of >97%, whereas the CoS_2 only show a specific capacity lower than 210 mA hg^{-1} (as shown in Fig. 4d).

As we have known, transition metal sulfide electrodes suffer a serious capacity fading because of the drastic volume change of the electrode during the conversion process [39] and the dissolution of lithium polysulfides in the electrolyte [2]. Furthermore, the smaller the particle size is, the less damage the electrodes undergoes during cycling. Therefore, the CoS_2 with size of 150 nm in CoS_2/RGO nanocomposites shows more stable cyclability than pristine CoS_2 with size of 2 μm. What's more, the elastic RGO nanosheets with high surface area inhibit the capacity decay by buffering volume changes during the lithium insertion and extraction processes and absorbing the lithium polysulfides [40–43]. According to previous work [41–43], the reduced graphene oxide (RGO) is used to envelope micron sized sulfur particles, to form a highly conductive network around the sulfur particles and trap the polysulfides through favorable hydrophilic–hydrophilic interactions.

Another considerable improvement is the rate capability of the CoS_2/RGO nanocomposites irrelative to the pristine CoS_2. As shown in Fig. 5a and b, the CoS_2/RGO nanocomposites show a much higher capacity than the pristine CoS_2 under all investigated current densities. The reversible capacity of CoS_2/RGO reached 720 mA hg^{-1}, 580 mA hg^{-1}, 330 mA hg^{-1}, 200 mA hg^{-1} when tested at 100 mA g^{-1}, 200 mA g^{-1}, 500 mA g^{-1}, 1000 mA g^{-1}, respectively. Importantly, after the high-rate measurements, the specific capacities of the CoS_2/RGO cycled under 100 mA g^{-1} were able to recover to the 550 mA hg^{-1}, implying their good reversibility [44]. In comparison, the pristine CoS_2 only delievered 100 mA hg^{-1} when tested at 500 mA g^{-1}. The good capacity

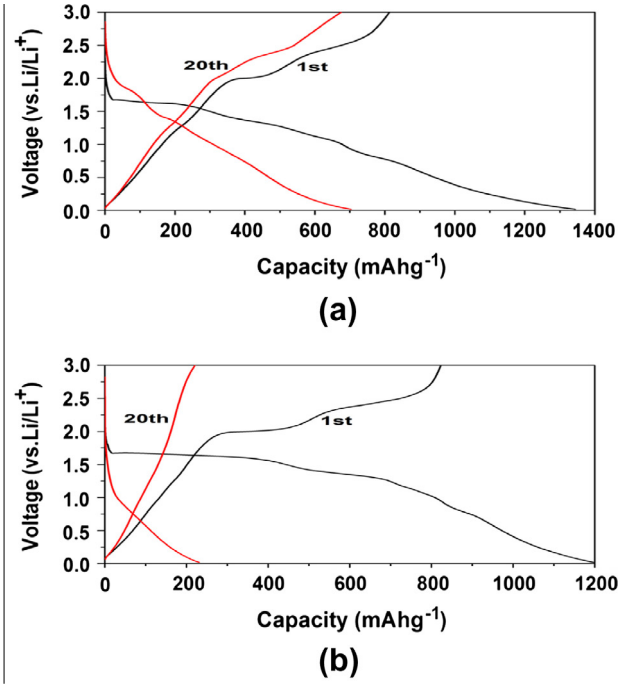

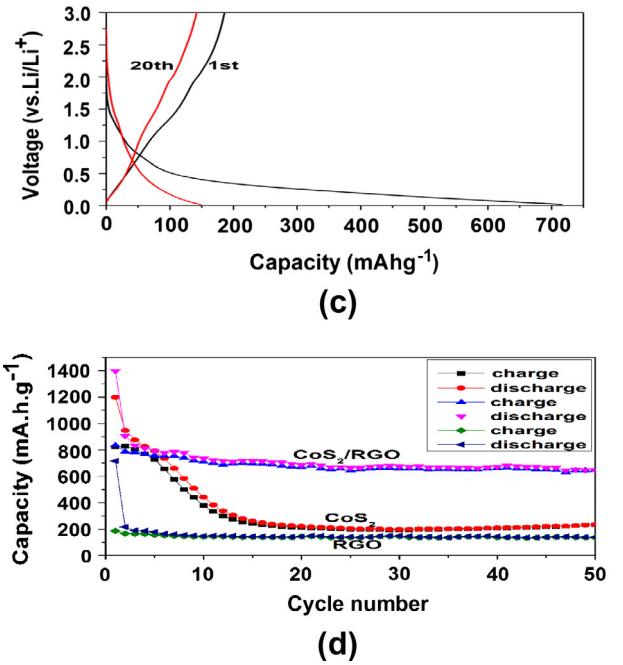

Fig. 4. (a) Charge-discharge curves of the CoS_2/RGO. (b) Charge-discharge curves of the CoS_2. (c) Charge-discharge curves of RGO. (d) Cycling performance of CoS_2, RGO and CoS_2/RGO.

retention and rate performance of the CoS_2/RGO may not only owe to the nanoscale particles but also the effects of RGO in preventing the agglomeration of CoS_2 and absorbing lithium polysulfides during the charge-discharge processes.

4. Conclusion

In summary, we have in situ synthesized CoS_2/RGO composites using GO as oxidizing agent and $Na_2S_2O_3$ as reducing agent. The CoS_2 particles with size of 150 nm are uniformly dispersed in the networks made from RGO nanosheets. As an anode material,

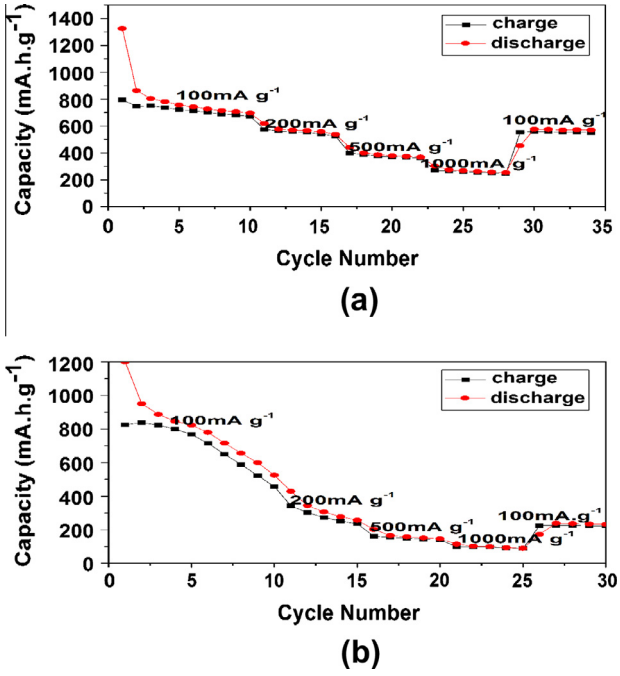

Fig. 5. (a) Cycling performance of CoS_2, CoS_2/RGO at various current densities. (b) Cycling performance of CoS_2 at various current densities.

CoS_2/RGO shows a higher specific capacity and batter rate performance than pristine CoS_2. The enhanced electrochemical behaviors can be attributed to the small particle size and elastic RGO with high surface area buffering the volume change and absorbing lithium polysulfides in the cycle process. The present work provides a new method to fabricate CoS_2/RGO nanocomposites, which can be extended to synthesis other metal sulfides (such as NiS, FeS_2, and MoS_2)/RGO composites to improve the cyclability and rate performance.

Acknowledgements

The authors acknowledge the financial supports from the major program of Beijing Municipal Natural Science Foundation (No. 20110001), National Natural Science Foundation of China (No. 11179001), National High Technology Research and Development Program (863, No. 2012AA052201).

References

[1] P.G. Bruce, S.A. Freunberger, L.J. Hardwick, J.M. Tarascon, Nat. Mater. 11 (2012) 19–29.
[2] J.F. Yin, H.Q. Cao, Z.F. Zhou, J.X. Zhang, M.Z. Qu, J. Mater. Chem. 22 (2012) 23963–23970.
[3] P.V. Prikhodchenko, J. Gun, S. Sladkevich, A.A. Mikhaylov, O. Lev, Y.Y. Tay, S.K. Batabyal, D.Y.W. Yu, Chem. Mater. 24 (2012) 4750–4757.
[4] P. Poizot, S. Laruelle, S. Grugeon, J.M. Tarascon, J. Electrochem. Soc. 149 (2002) A1212–A1217.
[5] G.B. Cho, K.W. Bae, T.H. Nam, J.H. Lee, J. Alloys Comp. 477 (2009) L24–L27.
[6] Y.J. Choi, N.W. Kim, K.W. Kim, K.K. Cho, G.B. Cho, H.J. Ahn, J.H. Ahn, K.S. Ryu, H.B. Gu, J. Alloys Comp. 485 (2009) 462–466.
[7] Y. Kim, J.B. Goodenough, J. Phys. Chem. C. 112 (2008) 15060–15064.
[8] J.Q. Dong, D.C. Li, Z.H. Peng, Y.H. Zhou, J. Solid State Electrochem. 12 (2008) 171–174.
[9] L. Zhang, H.B. Wu, X.W. Lou, Chem. Commun. 48 (2012) 6912–6914.
[10] M.R. Gao, Y.F. Xu, J. Jiang, S.H. Yu, Chem. Soc. Rev, doi: 10.1039/c2cs35310e.
[11] J. Xie, S.Y. Liu, G.S. Cao, T.J. Zhu, X.B. Zhao, Nano Energy 2 (2013) 49–56.
[12] G.C. Huang, T. Chen, Z. Wang, K. Chang, W.X. Chen, J. Power Sources, doi: 1016/j.jpowsour.2013.01.093.
[13] C. Xu, Y. Zeng, X.H. Rui, N. Xiao, J.X. Zhu, W.Y. Zhang, J. Chen, W.L. Liu, H.T. Tan, H.H. Hng, Q.Y. Yan, ACS Nano 6 (2012) 4713–4721.
[14] X.P. Fang, X.W. Guo, Y. Mao, C.X. Hua, L.Y. Shen, Y.S. Hu, Z.X. Wang, F. Wu, L.Q. Chen, Chem. Asian J. 7 (2012) 1013–1017.

[15] Q.H. Wang, L.F. Jiao, Y. Han, H.M. Du, W.X. Peng, Q.N. Huan, D.W. Song, Y.C. Si, Y.J. Wang, H.T. Yuan, J. Phys. Chem. C. 115 (2011) 8300–8304.
[16] Y.M. Wang, J.J. Wu, Y.F. Tang, X.J. Lu, C.Y. Yang, M.S. Qin, F.Q. Huang, X. Li, X. Zhang, ACS Appl. Mater. Interfaces 4 (2012) 4246–4250.
[17] X.Y. Zhao, D.G. Xia, K. Zheng, ACS Appl. Mater. Interfaces 4 (2012) 1350–1356.
[18] W. Luo, Y. Xie, C.Z. Wu, F. Zheng, Nanotechnology 19 (2008) 075602.
[19] Y.M. Liu, X.Y. Zhao, F. Li, D.D. Xia, Electrochim Acta. 56 (2011) 6448–6452.
[20] A.A. Farghali, M. Bahgat, W.M.A. El Rouby, M.H. Khedr, J. Alloys Comp. 555 (2013) 193–200.
[21] S.X. Min, G.G. Lu, J. Phys. Chem. C 116 (2012) 25415–25424.
[22] Y.Q. Zou, Y. Wang, ACS Nano 5 (2011) 8108–8114.
[23] Y. Wang, M.H. Wu, Z. Jiao, J.Y. Lee, Chem. Mater. 21 (2009) 3210–3215.
[24] K. Chang, W.X. Chen, Chem. Commun 47 (2011) 4252–4254.
[25] A. Kaniyoor, S. Ramaprabhu, J. Mater. Chem. 22 (2012) 8377–8384.
[26] J.J. Liang, Y. Huang, J.Y. Oh, M. Kozlov, D. Shi, S. Fang, R.H. Baughman, Y. Ma, Y.S. Chen, Adv. Funct. Mater. 21 (2011) 3778–3784.
[27] X.H. Chen, R. Fan, Chem. Mater. 13 (2001) 802–805.
[28] J.S. Jirkovsky, A. Bjorling, E. Ahlberg, J. Phys. Chem. C 116 (2012) 24436–24444.
[29] M. Zhang, S. Liu, X. Yin, Z. Du, Q. Hao, D. Lei, Q. Li, T. Wang, Chem. Asian J. 6 (2011) 1151–1154.
[30] I. Chakraborty, P.K. Malik, S.P. Moulik, J. Nanoparticle Res. 8 (2006) 889–897.
[31] S. Park, R.D. An, J.H.R.D. Piner, I. Jung, D.X. Yang, A. Velamakanni, S.T. Nguyen, R.S. Ruoff, Chem. Mater. 20 (2008) 6592–6594.
[32] A.C. Ferrari, J. Robertson, Phys. Rev. B 61 (2000) 14095–14107.
[33] W. Lin, K.S. Moon, S. Zhang, Y. Ding, J. Shang, M. Chen, C.P. Wong, ACS Nano 4 (2010) 1716–1722.
[34] W.F. Chen, L.F. Yan, P.R. Bangal, J. Phys. Chem. C 114 (2010) 19885–19890.
[35] Y.Y. Liang, D.Q. Wu, X.L. Feng, K. Mulle, Adv. Mater. 21 (2009) 1679–1683.
[36] J.M. Yan, H.Z. Huang, J. Zhang, Z.J. Liu, Y. Yang, J. Power Sources 146 (2005) 264–269.
[37] Q.H. Wang, L.F. Jiao, H.M. Du, W.X. Peng, Y. Han, D.W. Song, Y.C. Si, Y.J. Wang, H.T. Yuan, J. Mater. Chem. 21 (2011) 327–329.
[38] C.M. Ban, Z.C. Wu, D.T. Gillaspie, L. Chen, Y.F. Yan, J.L. Blackburn, A.C. Dillon, Adv. Mater. 22 (2010) E145–E149.
[39] M.T.S. Nair, Y. Pena, J. Campos, V.M. Garcia, P.K. Nair, J. Electrochem. Soc. 145 (1998) 2113–2120.
[40] Y.M. Sun, X.L. Hu, W. Luo, Y.H. Huang, J. Phys. Chem. C 116 (2012) 20794–20799.
[41] S. Evers, L.F. Nazar, Chem. Commun. 48 (2012) 1233–1235.
[42] S. Thakur, G. Das, P.K. Raul, N.J. Karak, J. Phys. Chem. C 117 (2013) 7636–7642.
[43] H.L. Wang, Y. Yang, Y.Y. Liang, J.T. Robinson, Y.G. Li, A. Jackson, Y. Cui, H.J. Dai, Nano Lett. 11 (2011) 2644–2647.
[44] G.M. Zhou, D.W. Wang, F. Li, L.L. Zhang, N. Li, Z.S. Wu, L. Wen, G.Q. Lu, H.M. Cheng, Chem. Mater. 22 (2010) 5306–5313.